Strain dynamics of influenza A

V Siska[a], M J Keeling[b]

[a]*Centre for Complexity Science, University of Warwick, Gibbet Hill Road, Coventry CV4 7AL, UK, V.Siska@warwick.ac.uk*
[b]*Department of Biological Sciences & Mathematics Institute, University of Warwick, Gibbet Hill Road, Coventry CV4 7AL, UK*

Abstract

We investigate the unusual observed patterns of influenza A strain dynamics in the northern hemisphere in the 2009/2010 and 2010/2011 influenza seasons, with particular attention to the US and the UK. During the 2009 pandemic, the novel A(H1N1)pdm09 strain, the so-called swine flu, dominated in both regions. Afterwards, the winter of 2010/2011 brought an overwhelming reinfection by the pandemic strain in Europe, but co-occurring epidemics of A(H1N1)pdm09 and a seasonal H3N2 strain in the US. Here we develop a single strain model with seasonal effects for the summer holidays and the winter months which can reproduce the two waves of the 2009/2010 season given there is a significant seasonal increase in transmission. A two-strain model with waning immunity, partial cross-immunity and prior immunity against the seasonal strain can display both UK-like and US-like behaviours, with the only difference being the initial conditions, namely, seeding and prior immunity.

Keywords: Epidemiology, Influenza, Cross-immunity, Waning immunity, Multiple strains, 2009 swine flu pandemic

Introduction

Influenza is an infectious disease of birds and mammals, spreading all over the world mainly in seasonal epidemics. Influenza A is of particular interest to modellers, due to the rich dynamics of its subtypes and strains and the now publicly available strain-specific data from surveillance schemes; serving commonly as a case study for the modelling of multi-strain pathogens.

Influenza A subtypes are classified based on the hemagglutinin (HA) and neuraminidase (NA) molecules, the antigenically active parts of the influenza A surface. As the primary antibody targets, these are under selection pressure from the immune system and mutate rapidly. Continuous changes, due to point mutations, are referred to as genetic drift. Drift leads to new virus strains capable of partially escaping pre-existing immunity in the population, acquired from prior infections. A genetic shift, on the other hand, refers to the introduction of a distinct HA or NA region in a virus. The resulting strain thus might be able to fully overcome prior immunity and cause a global pandemic.

The newly emerged A(H1N1)pdm09 strain, causing the first influenza pandemic of the 21st century in 2009, was the result of such a shift. It was the combination of an Eurasian 'avian-like' swine H1N1 strain and a North-American triple-reassortant strain, which carried genetic material from human seasonal H3N2, classical swine H1N1 and avian H1N1 strains (1).

The details of human immune response to the virus are still unclear, but evidence can be found for a rich variety of dynamics. Ferguson et. al. show that an immune response composing of a long-term strain-specific memory response and a short-term non-specific response is required to reproduce phylogenetic patterns as seen in sequence data (2). Mathews et. al consider two data sets showing a second wave, namely, the 1918 Spanish flu in RAF camps and an H3N2 outbreak on the island of Tristan de Cunha (TdC). Their study implies that pre-existing immunity plays an important role in the course of an epidemic, both by decreasing the chance of infection and mitigating the severity of symptoms, whereas waning immunity is needed to produce multiple waves (3). An other work of the TdC outbreak by Camacho et. al. implies that some hosts with either a delayed or deficient humoral immune response to the primary infection could be reinfected by the same strain (4).

By keeping track of the number of infectives of each strain and the history of susceptible hosts, one can formulate a natural multi-strain extension to the well-known SIR model. This approach has been used to model strains interacting through prohibiting superinfection by Dietz (5) or offering partial cross-immunity in an age-structured framework by Castillo-

Chavez et.al. (6). These works focused on two interacting strains and found conditions for stable coexistence when suitable invasion criteria are satisfied.

Further extensions of the model consider several strains, especially relevant for evolutionary epidemiology. Andreasen et. al. consider the history of susceptible individuals and the infection pressure for each strain (7) and show that sustained oscillations driven by cross-immunity can arise already for four interacting strains. Work by Gomes et. al. considers several strains with the same "fitness" in a circular strain-space, interacting through cross-immunity. They find that this system can self-organize into three different patterns, depending on the magnitude and distribution of cross-immunity: homogeneous or heterogeneous steady incidence or oscillatory dynamics with travelling waves in strain space (8). Gog & Grenfell formulate an alternative, status-based approach, greatly reducing the state space's dimensionality. This model also allows the investigation of antigenic drift and can produce emerging clusters of infection, resembling interpandemic influenza activity (9).

Our investigations were motivated by the unusual patterns observed following the 2009 (swine flu) pandemic. In the winter of 2010/2011, Europe experienced overwhelming infection by the pandemic H1N1 strain. In the UK in particular, influenza activity in these two years were of similar magnitude, while the burden of severe illness caused by influenza was even greater in the second year than in the pandemic year (10). The US, on the other hand, experienced infection by both the pandemic H1N1 and a seasonal H3N2 strain after the exclusive dominance of the pandemic strain in the season of 2009/2010 (11),(12).

An age-structure model based on the simple SIR model, with a variety of seasonal effects (different transmission rates for the seasons) and (waning and non-waning) prior immunity in order to explaining the three pandemic waves in the UK was formulated by Dorigatti et.al.. Heterogeneous immunity was assumed not to wane. They found that increased transmission in the third wave (2010/2011 season) was needed to reproduce the time-series, but other effects did not increase the quality of the fit substantially (13).

The purpose of this study is twofold. First, it attempts to investigate the role of temporal forcing and waning immunity in the three well-pronounced pandemic waves of swine flu in 2009 and 2010 in the UK. Second, it aims to explore some of the possible mechanisms to explain the qualitative difference in influenza A strain dominance between the UK and the US in the 2010/2011 influenza season.

Data

Influenza surveillance all over the world generally provides information on GP consultation rates and hospitalization rates, as well as virological data on strain dominance. The Centers for Disease Control and Prevention (CDC) publishes weekly surveillance reports for the United States as well as a summary at the end of each season. The Health Protection Agency (part of Public Health England) is responsible for weekly and annual summary reports on influenza activity over the United Kingdom. GP consultation and virological data fully covers these two countries, but hospitalization rates were limited for the USA. While laboratories and health care providers from all of the 50 states of the USA participated in the virological and outpatient surveillance systems, widely available hospitalization data is based on reports from only 13 states. We used virological and GP consultation data from annual summary reports in the US and the UK for the 2009/2010 and 2010/2011 seasons (Refs. (14), (15), (11) and (12)).

Description

Approximate time-series, based on GP consultation rates, are shown on Fig. 1. The rates are weighted according to the ratio of samples testing positive for the pandemic strain (H1N1) and the most common seasonal H3N2 strain. We can observe, that the pandemic strain was by far dominant in 2010, only interrupted in the summer months. The timing of the interruption coincides well with the timing of summer holidays in the given region. Summary statistics used in this study are shown in Tables A.1 and A.2. Wave sizes are obtained by the aggregation of corresponding data and growth rates from a naive linear fit on a logarithmic scale. These growth rates are in accordance with other estimates from different sources and areas (16).

It is also interesting to consider patterns in strain dominance on a longer time-scale. For this reason, we considered a public database maintained by WHO (FluNet), of laboratory-confirmed influenza-surveillance data by type and subtype (B, A(H3N2), A(H1N1), A(H1N1)pndm09). The proportion of samples for each category (Fig. 2) show the general trends, although small number of samples, especially for earlier years, makes the exact numbers uncertain. The general picture shows synchronisation for A(H3N2) between these two regions, as found in (17). However, in the year preceding the swine flu pandemic, different influenza A strains were dominant in the US and the UK: a seasonal H1N1 strain in the UK, but an H3N2 strain in the US.

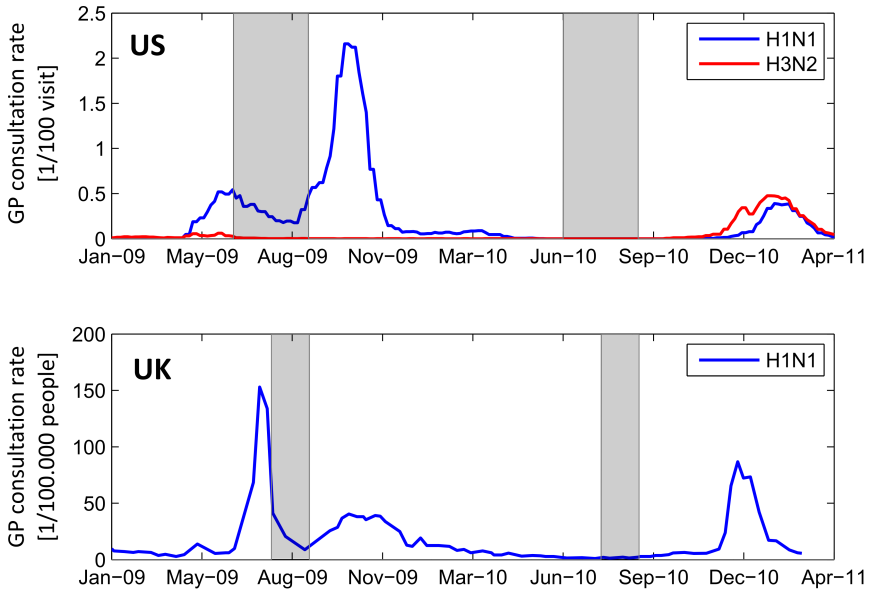

Figure 1: GP consultation rates for the US (top) and the UK (bottom) between 2009 April and 2010 April, multiplied by the proportion of samples positive for the pandemic H1N1 and seasonal H3N2 strains, corrected for type A samples not further subtyped. H3N2 incidence for the UK is not indicated, because it remained very low (under 2%) for these years. Grey areas indicate the summer school holidays.

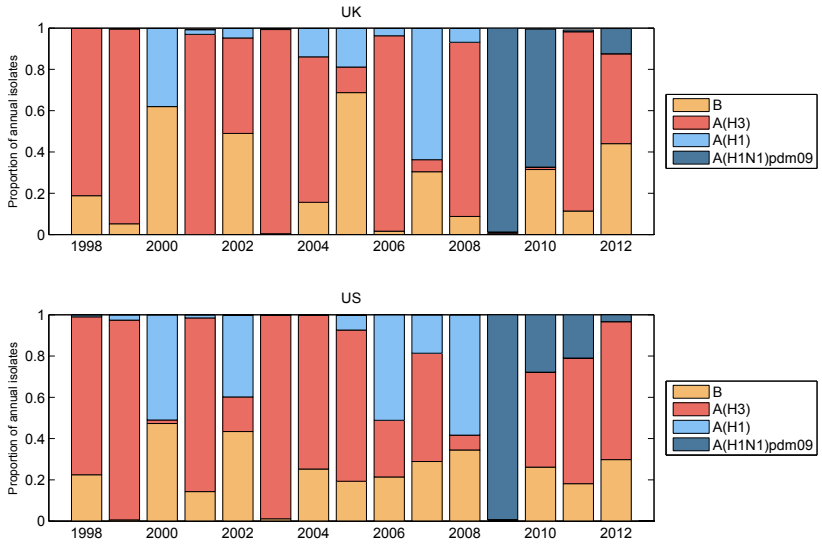

Figure 2: Proportion of annual isolates for the UK (top) and the US (bottom), plotted for each season from 1998/1999 to 2012/2013.

Limitations

There are various limitations in the data sources. First, the model produces incidence levels, whereas the best we can hope for in terms of the data, is time-series proportional to incidence. Often we don't quite get even that: the proportionality constant (e.g. reporting or hospitalization rates given infection) often substantially varies in time. Some typical sources of variability are the panic after the discovery of the new strain in Mexico; low public awareness in 2010 after the perceived overreaction to swine flu; changes in policy, such as the introduction of a novel telephone and internet based system (National Flu Service) during the 2009 autumn wave in the UK; or seasonal effects, like a higher rate of severe complications in harsh winter weather. As for the virological data, the quality also heavily depended on the number of samples collected and the efficiency of randomization.

An alarming sign of poor data quality is that different sources tell different stories. For instance, GP consultation rates for the UK show a large 2009 spring wave, a moderate 2009 autumn wave and a large 2010 autumn wave. Hospitalization data, on the other hand, imply similar waves in the spring and autumn of 2009 and a considerably larger and more abrupt peak starting in the autumn of 2010 (Fig. 3.). In general, hospitalization data is thought to be more accurate, as it depends less on the decision of individuals, but it is also less widely available.

Another limitation, more related to the simplicity of our model, is that we treated whole nations as well-mixed, homogeneous populations. No structure (e.g. spatial or population structure) was taken into account, not even for the US, and all data was aggregated per country.

Single strain

Model

The single-strain model was based on the simple SIR model, with added waning immunity and seasonality. The corresponding ODE system is shown on equation 1. It is worthwhile to mention that since we only considered a single pathogen for each subtype, waning immunity can be interpreted in two ways: either the immune response becoming deficient to prevent infection, or the given subtype drifting sufficiently to escape from prior immunity.

Two different seasonal effects were taken into account: decreased transmission during school holidays and increased transmission throughout the winter months, both represented as multipliers to the infection rate. A step function is the natural representative of school holidays, whereas for the winter months, the functional form makes no qualitative difference. We therefore decided to use the same step-function form for both, as shown on Fig. 4. A summary of all parameters of the model is shown in Table B.3.

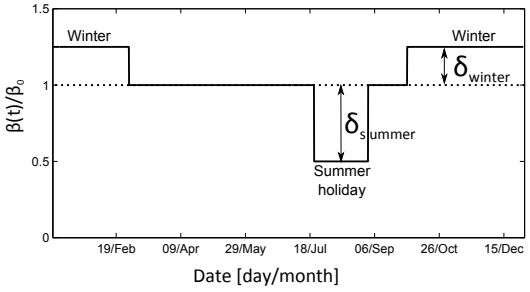

Figure 4: Functional form of seasonality used in the model.

$$\begin{aligned} \frac{dS}{dt} &= -\beta(t) S I + \omega R \\ \frac{dI}{dt} &= \beta(t) S I - \gamma I \\ \frac{dR}{dt} &= \gamma I - \omega R \end{aligned} \tag{1}$$

Results

We explored three versions of the model, with different seasonal effects for the winter months:

(i) No increased transmissibility.
(ii) Same increase in transmissibility in the winters of 2009/2010 and 2010/2011.
(iii) Increased transmissibility only for the winter of 2010/2011.
(iv) Different increase in transmissibility in the winters of 2009/2010 and 2010/2011.

The last two versions are similar to the model in (13), used to explain the third wave of infection by the pandemic H1N1 strain in the UK. Furthermore, we investigated both models in the absence of waning immunity.

Exploration of seasonality and waning immunity

Initially, we kept all parameters constant except for the magnitude of the seasonal increase in transmission, δ and the waning rate, ω. We chose the recovery rate γ to represent a biologically plausible recovery period for influenza (we made the same choice as (13)), the basic

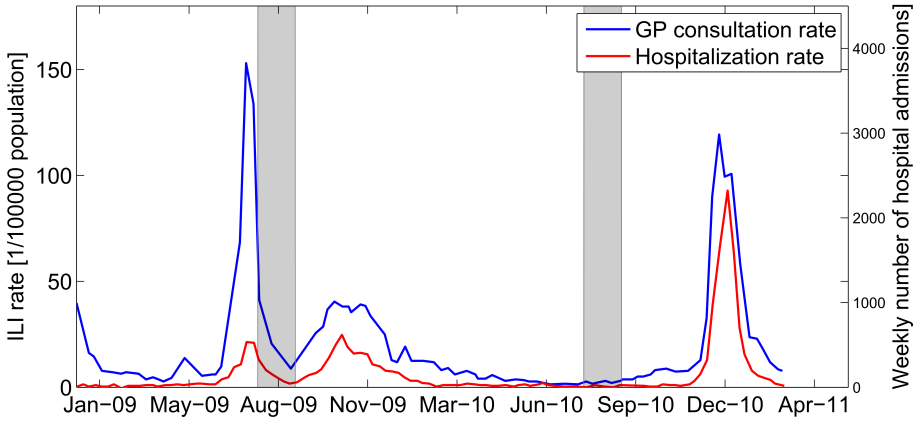

Figure 3: Hospitalization and GP consultation rates in the UK from 2009 January to 2011 April. Grey areas indicate the summer school holidays.

infection rate β_0 to reproduce growth rates as seen in the data and the drop in transmission rate for the school holidays to be in accordance with the decrease rate for the summer period. These constants are shown in Table B.4. Next, we performed a full parameter search on the rest of the parameters, namely δ and ω, for models (ii) and (iii) with waning immunity. As we will see, the added complexity for model (iv), with different transmission rates for each wave, hardly increased the level of agreement with the data. We chose the maximal waning rate (ω) to increase up to 1 per year for the model with increased transmission in only 2010 and up to 2 per year for the version with the same magnitude of increase. These limits were set to capture the parameter regime corresponding to the data but avoid multiple waves in a single season, not supported by the data. Seasonality was allowed to increase up to 0.5, again to capture the relevant behaviour.

The results (Figs. 5 and 6) show different behaviours for these two models and data sources. For the hospitalization data set, the model with the same magnitude of seasonality in both years struggles to reproduce the medium-sized autumn wave in 2009 followed by a large, steep peak next year. The model with increased transmissibility in 2010, on the other hand, can produce wave sizes as seen in the data. Results from the GP consultation rates are similar, but the model with the same amount of seasonality can also reproduce approximately correct wave sizes.

A further phenomenon worth mentioning, is the trade-off between waning immunity, increasing the susceptible pool, and increased transmission, increasing the infection rate; both increasing the effective reproductive ratio of the infection. One more interesting feature of the investigations is the emergence of an area with intermediate waning rate and low seasonal increase resulting in a small second, but large third wave for the model variant with the same increased transmission in both years. This is especially notable for the GP consultation data (Fig. 5, bottom-right panel) and corresponds to the second wave not taking off, leaving enough susceptibility for a third wave.

Reproducing time-series

To verify the previous observations, we also attempted to fit time-series of hospitalization and GP consultation rates for the UK, despite the data sources' limitations. Euclidean distance from the data was used as a cost function, since the number of cases was large. We integrated the ODEs using the Runge-Kutta method in Matlab R2011b and applied Matlab's `fminsearch` algorithm to search for an optimum. `fminsearch` is a non-gradient-based method utilizing the simplex method ((18)). Such a tool is useful for such a non-smooth fitness landscape, with high sensitivity to seeding through the timing of the peaks.

The obtained results from model variants with waning immunity, as shown in Table B.5 and Fig. 8, were in accordance with previous observations: the fit was satisfying for different infection rates and model types, but some form of increase in transmission was required for a good fit. As was already visible during the exploration, model (ii) with the same level of seasonality struggled to produce such a dominant third wave as seen in the hospitalization data. The ILI data, on the other hand, favoured model (ii). It was interesting to observe that the fit to neither of the data sources saw a remarkable improvement when the infection rate was allowed to be

different for all three waves.

It is worthwhile to note the wide range of waning rates corresponding to the best-fitting models. While models with an increased transmission rate in 2010 favoured lower waning rates (ω = 0.0008/day and ω = 0.0002/day, corresponding to average waning periods of 3.5 years and 13.5 years for the hospitalization and GP consultation data, respectively), immunity waned much quicker in those with the same magnitude of seasonality in both years (0.0048/day and 0.0024/day, corresponding to average waning periods of 0.5 year and 1 year for the hospitalization and GP consultation data, respectively). The latter values are too high, marked also by the slight rise in incidence in the summer of 2010, clearly visible for the variant using the hospitalization data. Such oscillatory behaviour in a single season is not typical for influenza, but would possibly be suppressed by a smooth representation of the seasonal increase even in our model.

The magnitude of seasonal increase in transmission for the winter months also varied between different models and data sources. For models (iii) and (iv) without waning immunity (the only two variants that produced three waves in the absence of this effect), δ_{winter} for the 2010/2011 season was high, ranging from 70% to 310% (Table B.6). Some model variants required a similarly high increase in transmission for the third wave even with waning immunity. These were models (iii) and (iv) for the hospitalization data and (iii) for the GP consultation data. On the other hand, variant (ii) for the hospitalization and variants (ii) and (iv) for the GP consultation data could produce three waves even with a smaller seasonal effect, with the magnitude of additional infection rate between 20% and 36% (Table B.5).

As a further investigation, the model was also fitted to the time-series in absence of waning immunity (Fig. B.6 and Fig. 7). This variant required increased transmission in the third season for a third wave to occur, similar to the result of (13). In accordance with our observations with the model variant with waning immunity and also with those of (13), the quality of the fit hardly improved when different transmission rates were allowed for all three waves.

Two interacting strains

Model

We chose to work with a standard history-based model and omitted super-infection or co-infection by the two strains. The former is limited by neuraminidase as part of the cell based secondary immune system (19) and the latter is thought to be existing, but rare (20). Cross-immunity was represented as decreased susceptibility for a strain after having recovered from the other. An alternative mechanism would have been decreased infectivity, but these two approaches act in the same way for two strains and lead to similar results even for many strains (21). The final assumption was that strain-specific immunity wanes independently. An illustration of the model is shown on Fig. 9a., while the corresponding system of ordinary differential equations are described in Eq. 2.

The general behaviour of the model is as follows. Stable co-existence is possible if appropriate invasion criteria are satisfied, corresponding to weak cross-immunity and the reproductive ratios of the pathogens being close enough (22). The transient behaviour, however, can show rich dynamics, based on the time-scales and reproductive ratios of the two pathogens and the degree of cross-protection. These include multiple peaks separated in time, one strain suppressed by the other or simultaneous epidemics by both strains. Seasonality further complicates the variety of scenarios but the length of this study does not permit us to conduct a full investigation. We will instead focus on the model's ability to reproduce the main characteristics of our data.

A minor modification to the model was also investigated, namely, a short-term heterogeneous immunity. Individuals in this model were first transferred to a class totally protected from any strain before arriving at their respective recovered class. An illustration of this variant is shown on Fig. 9b.

$$
\begin{aligned}
\frac{dN_{SS}}{dt} &= \omega N_{RS} + \omega N_{SR} - \\
&\quad -N_{SS}\left(\beta_1\left(N_{IS}+N_{IR}\right)+\beta_2\left(N_{S1}+N_{RI}\right)\right) \\
\frac{dN_{IS}}{dt} &= N_{SS}\beta_1\left(N_{IS}+N_{IR}\right) - \gamma N_{IS} \\
\frac{dN_{RS}}{dt} &= \gamma N_{IS} - N_{RS}\sigma\beta_2\left(N_{S1}+N_{RI}\right) + \\
&\quad +\omega N_{RR} - \omega N_{RS} \\
\frac{dN_{S1}}{dt} &= N_{SS}\beta_2\left(N_{S1}+N_{RI}\right) - \gamma N_{S1} \\
\frac{dN_{RI}}{dt} &= N_{RS}\sigma\beta_2\left(N_{S1}+N_{RI}\right) - \gamma N_{RI} \\
\frac{dN_{SR}}{dt} &= \gamma N_{S1} - N_{SR}\sigma\beta_1\left(N_{S1}+N_{RI}\right) + \\
&\quad +\omega N_{RR} - \omega N_{SR} \\
\frac{dN_{IR}}{dt} &= N_{SR}\sigma\beta_1\left(N_{IS}+N_{IR}\right) - \gamma N_{IR} \\
\frac{dN_{RR}}{dt} &= \gamma N_{IR} + \gamma N_{RI} - 2\omega N_{RR}
\end{aligned}
\tag{2}
$$

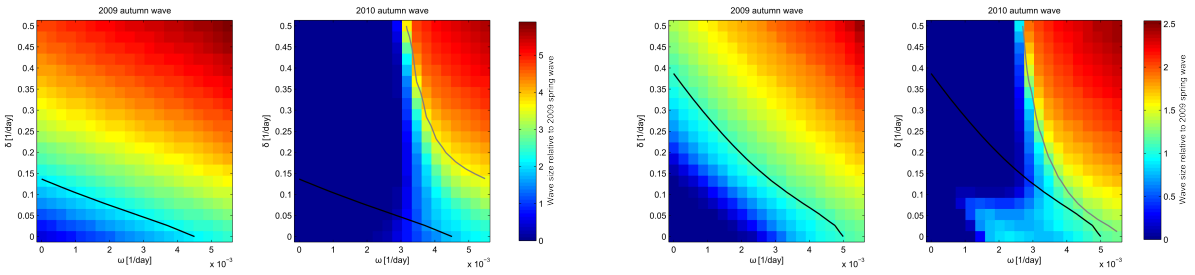

(a) Hospitalization data

(b) GP consultation data

Figure 5: Results for variant (ii), with the same seasonality in both years, based on hospitalization (5a) and GP consultation (5b) data. Sizes of the autumn waves in 2009 (left) and 2010 (right) relative to the 2009 spring wave are color coded and shown as a function of waning rate ω and winter seasonality δ. All other parameters were fixed to reproduce the 2009 spring wave, with values as in Table B.4. Wave sizes from the data are displayed as black (autumn 2009) and grey (autumn 2010) lines.

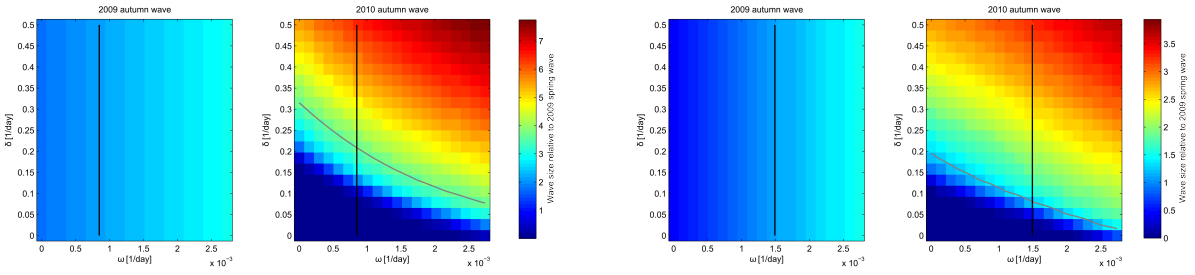

(a) Hospitalization data

(b) GP consultation data

Figure 6: Results for variant (iii), with seasonality only in the the winter of 2010/2011, based on hospitalization (6a) and GP consultation (6b) data. Sizes of the autumn waves in 2009 (left panels) and 2010 (right panels) relative to the 2009 spring wave are color coded and shown as a function of waning rate ω and winter seasonality δ. All other parameters were fixed to reproduce the 2009 spring wave, with values as in Table B.4. Wave sizes from the data are displayed as black (autumn 2009) and grey (autumn 2010) lines.

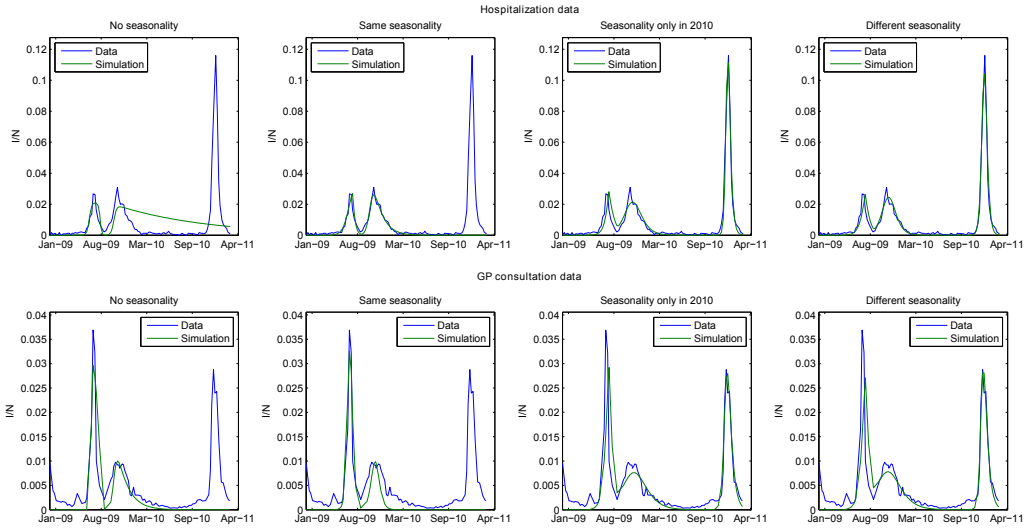

Figure 7: Fitting to the time-series from hospitalization (top row) and GP consultation (bottom row) data, without waning immunity and different seasonal effects. Types of seasonal effects, as organized by coloumns from left to right, are as follows: no increase in transmission, same magnitude of increased transmission in 2009 and 2010, increased transmission only in 2010, and different magnitudes of increased transmission in 2009 and 2010.

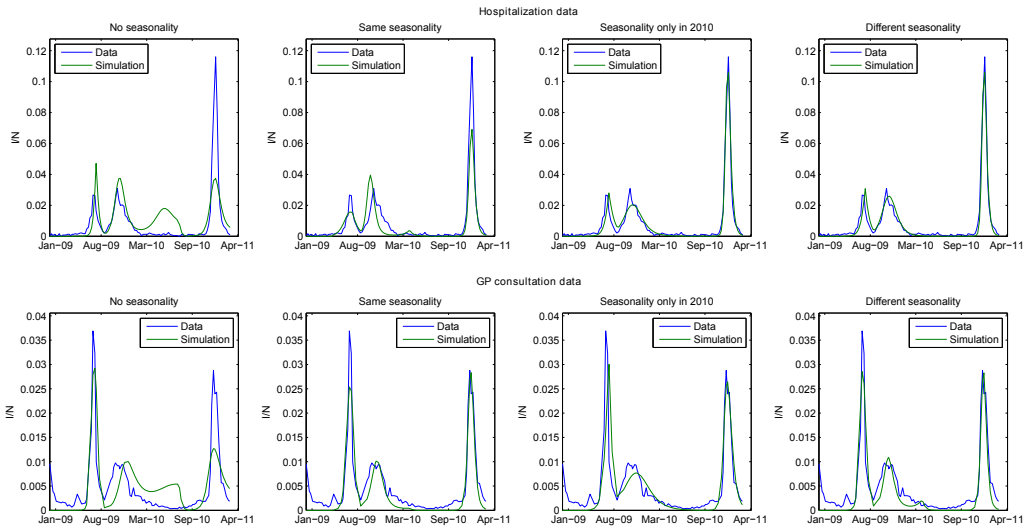

Figure 8: Fitting to the time-series from hospitalization (top row) and GP consultation (bottom row) data, with waning immunity. Types of seasonal effects, as organized by coloumns from left to right, are as follows: no increase in transmission, same magnitude of increased transmission in 2009 and 2010, increased transmission only in 2010, and different magnitudes of increased transmission in 2009 and 2010.

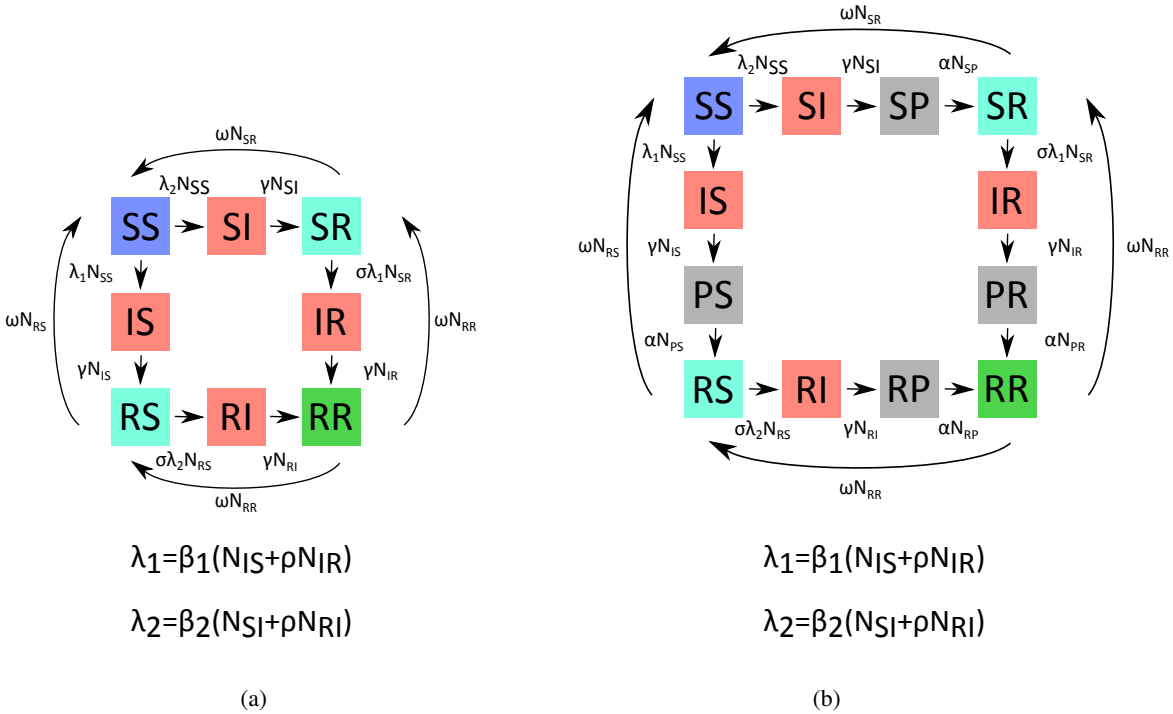

Figure 9: Illustration of the two-strain model with (9a) and without (9b) short-term immunity.

We were only considering two influenza A strains, similar in nature. Therefore, all parameters were set to be equal, except for infection rates β^1 and β^2, in order to account for variability in transmissibility.

We used data from GP consultation rates while fitting for both strains, since they were readily available from the same areas as the virological data. Due to the large uncertainties in the data, we decided to use only the sizes of the waves relative to the 2009 autumn wave, which was well pronounced in both regions.

A summary of all parameters of the model are shown on Table C.7. First, all parameters were estimated, but since the resulting simulations often had an unrealistic shape, namely, very large growth rates, and the number of parameters was very high, we decided to take initial growth rates of the pandemic into account as well. In this model variant, the recovery rate was fixed to a biologically plausible value for influenza, and the infection rate for the pandemic strain was set to reproduce the growth rate of the 2009 spring wave from GP consultation data in the UK (0.0888/day, number of cases doubling approximately every 8 days). The growth rate r_0 in the presented two-strain model and notation, for one of the strains, is as follows:

$$r_0^1 = \beta_1 \left(N_{SS} + \sigma N_{SR}\right) - \gamma \tag{3}$$

We integrated the ODEs using the Runge-Kutta method in Matlab R2011b and Matlab's gradient-based `GlobalSearch` tool for minimizing the Euclidean distance between the data and the model output (18). The choice of optimization method was based on performance, after experimenting with Matlab's `fminsearch` and `GlobalSearch` algorithms as well as a self-implemented evolutionary algorithm and simulated annealing.

Results

At the start of the 2009 spring wave, individuals were assigned to the four disease-free compartments. Without waning immunity, the model could not reproduce the data even if all parameters were allowed to vary and converged to a case with only the pandemic strain present for all model variants instead.

The model variant with fixed growth rate and recovery rate managed to reproduce the data, given some prior immunity against the seasonal strain. The best-fitting parameter sets are given in Table C.8, while the resulting wave sizes are shown on Figs. 10a to 10d. The

shape of the time-series was somewhat different from what is seen in the data (Figs. 11a and 11b), possibly caused by the non-smooth functional form for seasonality.

The best-fitting parameter set without prior immunity did not manage to produce correctly sized waves, whereas the variant with immunity only against the pandemic strain resulted in no prior immunity at all and similarly bad fit. When prior immunity was allowed only against the non-pandemic H3N2 strain, the quality of the fit was high, with all wave sizes approximately correct. The best fitting parameter set consisted of biologically plausible parameters and initial conditions. In particular, immune levels against the non-pandemic strain in the UK ($\approx$ 72 %) exceeded that in the US ($\approx$ 60 %), which seems biologically plausible, given that a seasonal H3N2 strain was dominant in the 2008/2009 influenza season in the UK and an H1N1 strain in the same season in the US.

When all initial conditions were fitted, the quality of the fit improved slightly even more. The best fitting parameters for the US had lower levels of prior immunity than those for the UK, both against the pandemic strain ($N_{N_RS} + N_{RR} \approx 31\%$ as opposed to $N_{N_RS} + N_{RR} \approx 34\%$), and the seasonal H3N2 strain ($N_{N_SR} + N_{RR} \approx 80\%$ in contrast with $N_{N_SR} + N_{RR} \approx 87\%$). The latter was expected, but the former is in contrast with previous epidemiological history of the two regions. However, the differences are to small to draw any firm conclusion.

The general pattern of higher pre-existing immunity in the UK than in the US could have been a consequence of prior immunity decreasing the final proportion of recovered individuals in a population after a single epidemic. Therefore, a high immune level in 2009 spring decreases immune levels by the start of the 2010 season, permitting a larger epidemic by the same strain, as it happened in the UK. The interruption by school holidays has a similar effect, but that was present in both regions.

Well-fitting parameter sets had high levels of cross-reactivity, equivalent to low levels of remaining susceptibility: approximately 24% and 37% for variants with pre-existing immunity against the seasonal or both strains, respectively. They also had low waning rates: 0.0008 and 0.0005, corresponding to average waning times of around 3.5 years and 5.5 years for these two models. The seasonal increase in transmissibility for well-fitting models was intermediate; roughly 50% and 80% for the models with prior immunity against H3N2 or both strains, respectively.

It is worthwhile to note that if all parameters were estimated and the limits were generous enough, correct wave sizes could be reproduced even without prior immunity. However, when started from random initial conditions, this model variant converged to parameter sets with unrealistically high growth rates (at least 1.7/day, about twice as much as in the data) and, in some cases, high recovery rates as well. When started from the optimum of the constrained model, it remained close to the initial condition with a final cost close to the initial value (within 20%).

A further remark is that the model variant with short-term heterogeneous immunity did not increase the quality of the fit to the data substantially. The optimization method favoured the waning rate for this effect being close to the lowest allowed value and the values of the cost function were similar to those without the added effect (never more than 10% less).

Once we obtained some models capable of reconstructing waves similar to the data, we very briefly had a look at their long-term behaviour. The time-series seemed to reach an equilibrium, but the nature of this equilibrium was sensitive to the exact parameter set. Some examples from the best-fitting parameter sets with fixed growth rate and recovery rate and prior immunity against the seasonal strain or both strains are shown on Figs. 11a and 11b, respectively. These models show a two-year pattern of epidemics, with an alternating dominant strain, not unlike general seasonal influenza patterns. In reality, in 2011, the normal seasonal epidemic was nearly absent in the UK, before the seasonal H3N2 strain returned, but this particular behaviour is not captured by our simple model. As for the US, both the pandemic H1N1 and the seasonal H3N2 strains were present in subsequent years, similar to the long-term behaviour of our best-fitting models.

Discussion

These very simple models applied to data from the 2009/2010 and 2010/2011 influenza seasons managed to reproduce the main trends seen in the data. The one-strain model showed that some form of seasonality (either in both years or for only 2010) was needed to reproduce three distinct waves of the pandemic strain, as seen in the UK. Most model variants required a large increase in transmission, but some with waning immunity and seasonality in both years produced realistic results even with a weaker seasonal effect. Furthermore, school holidays played an important role in shaping the pandemic in 2009, starting in spring, an unusual time for influenza. An interesting trade-off between waning immunity and the seasonal increase could also be ob-

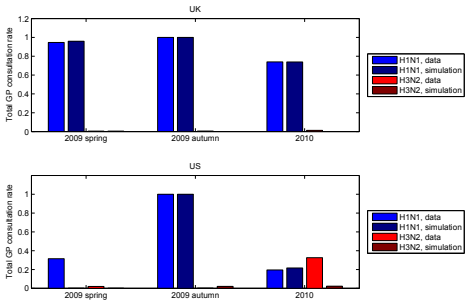

(a) No prior immunity

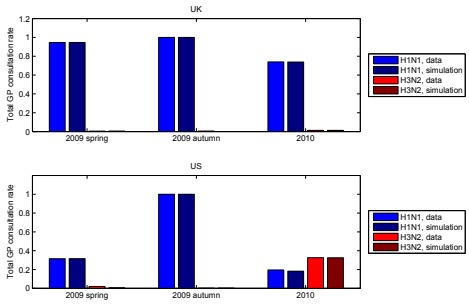

(b) Prior immunity only against the seasonal H3N2 strain.

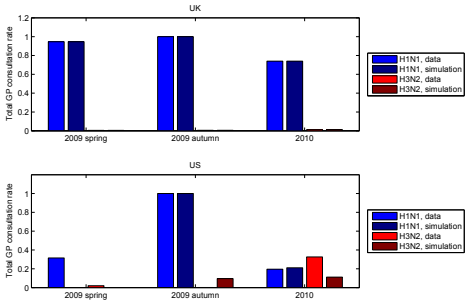

(c) Prior immunity only against the pandemic H1N1 strain.

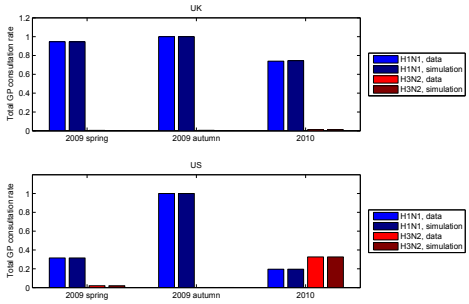

(d) Prior immunity against both strains.

Figure 10: Wave sizes from the best-fitting model for the UK and the US between 2009 April and 2010 April, with fixed growth rate and recovery rate and various constraints on prior immunity.

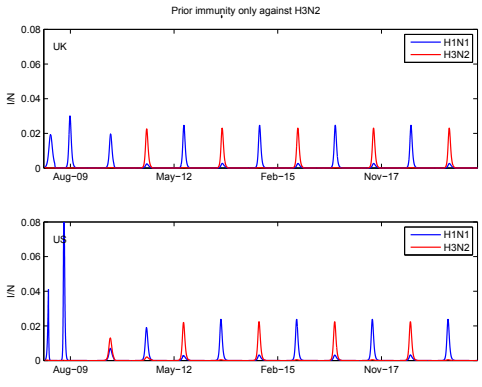

(a) Prior immunity only against the seasonal H3N2 strain.

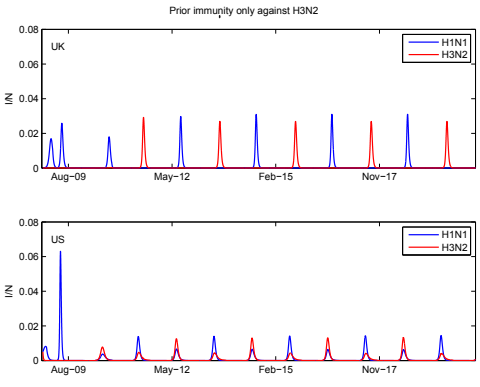

(b) Prior immunity against both strains.

Figure 11: Long-term behaviour of the best-fitting model for the UK and the US between 2009 April and 2010 April, with fixed growth rate and recovery rate and prior immunity only against the seasonal H3N2 strain (11a) or both strains (11b).

served, where the replenishment of susceptibles play the same role as an increase in the infection rate.

The two-strain version of the model showed both UK-like and US-like behaviours, switching between the two by changing only the initial conditions (seeding and pre-existing immunity) and the timing of school holidays. Unless growth rates were allowed to be unrealistically high, prior immunity was necessary to achieve correctly sized waves. Agreement with the data was satisfactory even if the population was assumed to be totally susceptible to the pandemic strain and levels of immunity were in accordance with previous epidemiological history of the two regions. Prior immunity against the pandemic strain further increased the quality of the fit, although also resulted in immunity patterns slightly contradicting the patterns of strain dominance from previous seasonal influenza epidemics. An intermediate increase in transmission during the winter months was enough for both versions of the model: roughly 50% and 80% for variants with prior immunity only against H3N2 or both strains, respectively.

Our models suffer from numerous limitations. No spatial structure was taken into account, which is a very crude approximation, especially for the US. Furthermore, no age-structure or demographic processes were included. Vaccination was also not modelled, even though a vaccine was made available and used even before the pandemic year, unlike previous pandemics. Vaccination coverage reached significant proportions, especially in the elderly and at-risk cohorts, by administering about 5.5 million doses in 2009/2010 and 9 million doses in 2010/2011 in England (23), (24); and around 80 million doses in 2009/2010 and 130 million doses in 2010/2011 in the US (25), (26). Futhermore, only two strains and simple dynamics of immunity were taken into account, despite the rich dynamics of influenza.

Strain-specific epidemiological modelling is a vast field, offering many perspectives with regards to our model. First, it could be extended to a more realistic form, or even complemented with additional immunological mechanisms, although one would have to take care not to overcomplicate the model, given the poor quality of the data. A simpler modification would be simply to allow some other parameters to differ between the two strains or the two regions. Second, the long-term behaviour of this model could be investigated in more detail, either by examining the result of numerical integration, or by constructing a discrete-time model consisting of prior immunities at, say, the beginning of each season. Third, considering other countries, such as other European countries with UK-like behaviour but US-like school holidays, or Australia with the onset of the pandemic in the normal influenza season, could strengthen our conclusions.

References

[1] G. J. Smith, D. Vijaykrishna, J. Bahl, S. J. Lycett, M. Worobey, O. G. Pybus, S. K. Ma, C. L. Cheung, J. Raghwani, S. Bhatt, et al., Origins and evolutionary genomics of the 2009 swine-origin h1n1 influenza a epidemic, Nature 459 (7250) (2009) 1122–1125.

[2] N. M. Ferguson, A. P. Galvani, R. M. Bush, Ecological and immunological determinants of influenza evolution, Nature 422 (6930) (2003) 428–433.

[3] J. D. Mathews, C. T. McCaw, J. McVernon, E. S. McBryde, J. M. McCaw, A biological model for influenza transmission: pandemic planning implications of asymptomatic infection and immunity, PLoS One 2 (11) (2007) e1220.

[4] A. Camacho, S. Ballesteros, A. L. Graham, F. Carrat, O. Ratmann, B. Cazelles, Explaining rapid reinfections in multiple-wave influenza outbreaks: Tristan da cunha 1971 epidemic as a case study, Proceedings of the Royal Society B: Biological Sciences 278 (1725) (2011) 3635–3643.

[5] K. Dietz, Epidemiologic interference of virus populations, Journal of mathematical biology 8 (3) (1979) 291–300.

[6] C. Castillo-Chavez, H. Hethcote, V. Andreasen, S. Levin, W. M. Liu, Epidemiological models with age structure, proportionate mixing, and cross-immunity, Journal of mathematical biology 27 (3) (1989) 233–258.

[7] V. Andreasen, J. Lin, S. A. Levin, The dynamics of cocirculating influenza strains conferring partial cross-immunity, Journal of mathematical biology 35 (7) (1997) 825–842.

[8] M. G. M. Gomes, G. F. Medley, D. J. Nokes, On the determinants of population structure in antigenically diverse pathogens, Proceedings of the Royal Society of London. Series B: Biological Sciences 269 (1488) (2002) 227–233.

[9] J. R. Gog, B. T. Grenfell, Dynamics and selection of many-strain pathogens, Proceedings of the National Academy of Sciences 99 (26) (2002) 17209–17214.

[10] O. Mytton, P. Rutter, L. Donaldson, et al., Influenza a (h1n1) pdm09 in england, 2009 to 2011: a greater burden of severe illness in the year after the pandemic than in the pandemic year, Euro Surveill 17 (14) (2012) 20139.

[11] Centers for Disease Control and Prevention Influenza Division, Fluview 2009-2010 influenza season summary, `http://www.cdc.gov/flu/weekly/weeklyarchives2009-2010/09-10summary.htm`, accessed 12 February 2014 (November 2011).

[12] Centers for Disease Control and Prevention Influenza Division, Fluview 2010-2011 influenza season summary, `http://www.cdc.gov/flu/weekly/weeklyarchives2010-2011/10-11summary.htm`, accessed 12 February 2014 (January 2010).

[13] I. Dorigatti, S. Cauchemez, N. M. Ferguson, Increased transmissibility explains the third wave of infection by the 2009 h1n1 pandemic virus in england, Proceedings of the National Academy of Sciences 110 (33) (2013) 13422–13427.

[14] Health Protection Agency, Epidemiological report of the pandemic (h1n1) 2009 in the uk, `http://www.hpa.org.uk/Publications/InfectiousDiseases/Influenza/1010EpidemiologicalreportofpandemicH1N12009inUK/`, accessed 12 February 2014 (October 2010).

[15] Health Protection Agency, Surveillance of influenza and other respiratory viruses in the uk: 2010-2011 report, `http:`

//www.hpa.org.uk/web/HPAweb&HPAwebStandard/HPAweb/C/1296687412376, accessed 12 February 2014 (May 2011).

[16] P.-Y. Bolle, S. Ansart, A. Cori, A.-J. Valleron, Transmission parameters of the a/h1n1 (2009) influenza virus pandemic: a review, Influenza and Other Respiratory Viruses 5 (5) (2011) 306–316. doi:10.1111/j.1750-2659.2011.00234.x.
URL http://dx.doi.org/10.1111/j.1750-2659.2011.00234.x

[17] B. S. Finkelman, C. Viboud, K. Koelle, M. J. Ferrari, N. Bharti, B. T. Grenfell, Global patterns in seasonal activity of influenza a/h3n2, a/h1n1, and b from 1997 to 2005: viral coexistence and latitudinal gradients, PloS one 2 (12) (2007) e1296.

[18] The MathWorks, Inc., Optimization Toolbox^{TN} User's Guide, r2013b Edition, http://www.mathworks.com/help/releases/R2013b/pdf_doc/optim/optim_tb.pdf (September 2013).

[19] I.-C. Huang, W. Li, J. Sui, W. Marasco, H. Choe, M. Farzan, Influenza a virus neuraminidase limits viral superinfection, Journal of virology 82 (10) (2008) 4834–4843.

[20] M. Peacey, R. J. Hall, S. Sonnberg, M. Ducatez, S. Paine, M. Nicol, J. C. Ralston, D. Bandaranayake, V. Hope, R. J. Webby, et al., Pandemic (h1n1) 2009 and seasonal influenza a (h1n1) co-infection, new zealand, 2009, Emerging infectious diseases 16 (10) (2010) 1618.

[21] N. Ferguson, V. Andreasen, The influence of different forms of cross-protective immunity on the population dynamics of antigenically diverse pathogens, in: Mathematical approaches for emerging and reemerging infectious diseases: models, methods, and theory, Springer, 2002, pp. 157–169.

[22] M. J. Keeling, P. Rohani, Modeling infectious diseases in humans and animals, Princeton University Press, 2008.

[23] Health Protection Agency, Pandemic h1n1 (swine) influenza vaccine uptake amongst patients groups in primary care in england., https://www.gov.uk/government/uploads/system/uploads/attachment_data/file/215977/dh_121014.pdf, accessed 20 June 2014 (October 2010).

[24] Health Protection Agency, Pandemic h1n1 (swine) influenza vaccine uptake amongst patients groups in primary care in england., https://www.gov.uk/government/uploads/system/uploads/attachment_data/file/216393/dh_129856.pdf, accessed 20 June 2014 (May 2011).

[25] Centers for Disease Control and Prevention Influenza Division, Final estimates for 200910 seasonal influenza and influenza a (h1n1) 2009 monovalent vaccination coverage united states, august 2009 through may, 2010., http://www.cdc.gov/flu/fluvaxview/coverage_0910estimates.htm, accessed 20 June 2014 (November 2011).

[26] Centers for Disease Control and Prevention Influenza Division, Final state-level influenza vaccination coverage estimates for the 201011 seasonunited states, national immunization survey and behavioral risk factor surveillance system, august 2010 through may 2011, http://www.cdc.gov/flu/fluvaxview/coverage_1011estimates.htm, accessed 12 February 2014 (January 2010).

Appendix A. Summary statistics for the data

Due to the poor data quality and an unknown proportionality constant present in both data sources, we had to rely on summary statistics to compare our model to the observed dynamics. The first table (Table A.1) shows summary statistics for the UK from hospitalization and GP consultation data, used in the study of our single strain model. The second table focuses on characteristics of strain-specific data from GP consultation rates in the US and the UK, utilized in the investigation of our two-strain model (Table A.2).

Table A.1: Summary statistics of the two different data sources for the UK. All wave sizes are relative to the size of the 2009 spring wave. Growth and decrease rates are computed from a linear fit to the logarithm of the data.

	Hospitalization	GP consultation
2009 autumn wave size	2.1287	1.0829
2010 autumn wave size [1/day]	3.6345	1.2536
2009 spring growth rate [1/day]	0.0718	0.0888
2009 summer decrease rate [1/day]	0.0506	0.0589

Table A.2: Wave sizes for the two strains (pandemic H1N1 and seasonal H3N2) in the two regions (US and UK), for the three waves (2009 spring, 2009 autumn, 2010 autumn), relative to the 2009 autumn wave of the pandemic H1N1 strain.

UK	H1N1	H3N2
2009 spring	0.9466	0.0048
2009 autumn	1.0000	0.0051
2010 autumn	0.7399	0.0123

US	H1N1	H3N2
2009 spring	0.3150	0.0198
2009 autumn	1.0000	0.0011
2010 autumn	0.1957	0.3261

Appendix B. Parameter values for the single strain model

Tables summarizing parameter values for the single strain model are shown below, with all parameters explained on Table B.3. Most parameters were fixed during the exploration of variant (ii), with the same magnitude of seasonality in both years; and variant (iii), with increased transmission in both years. The values of these constants are shown in Table B.4. The recovery rate γ was fixed at a biologically plausible value, from Ref. (13). The infection rate β was set to produce the correct (exponential) growth rate, calculated as $r_0 = \beta - \gamma$. The decrease in transmission during the summer holidays, δ_{summer}, was chosen such that the (exponential) decrease rate, $r_0 = (1 + \delta_{summer})\beta - \gamma$ was as seen in the data. The values for these rates as estimated from the data are shown in Table A.1. The initial fraction of infectives (seed) for the spring wave was chosen to produce wave sizes that include the observed values within the explored parameter set. Since we were only interested in the size of each wave during this exploration, the seeding for the next year did not matter, as long as the bulk of the 2010 autumn wave fell within the 2010/2011 influenza season.

Tables B.5 and B.6 show the best-fitting parameter sets from fitting the four variants of the model to time-series from GP consultation rates and hospitalization rates. The dynamics during low-incidence periods are governed by processes not included in our model, such as the spatial spread between different regions or stochasticity. Therefore, the only role of seeds is to set the timing of peaks. For instance, small negative seeds, although biologically meaningless, delay the onset of the epidemic.

Table B.3: Summary of model parameters for the single-strain model.

Notation	Parameter	Value for exploration	Value for fitting
β	Infection rate [1/day]	fixed	estimated
γ	Recovery rate [1/day]	fixed	estimated
ω	Waning rate [1/day]	estimated	estimated or fixed
δ_{summer}	Additional infection rate relative to base level for the summer holidays	fixed	estimated
δ^1_{winter}	Additional infection rate relative to base level for the winter months in 2009	estimated	estimated or fixed
δ^2_{winter}	Additional infection rate relative to base level for the winter months in 2010	estimated	estimated or fixed
i_1	Initial proportion of infectives in the beginning of 2009 spring wave (April 20)	fixed	estimated
i_2	Initial proportion of infectives in the beginning of 2010 autumn wave (September 10)	fixed	estimated

Table B.4: Fixed parameters used during the exploration of variants (ii) and (iii) of the single-strain model, for the two data sources.

Data source	*beta*	γ	δ_{summer}	i_1	i_2
Hospitalization	0.4117	0.3548	-0.0153	1.15e-04	0
GP consultation	0.4367	0.3548	-0.3224	8.00e-05	0

Table B.5: Best-fitting parameter sets for all four variants of the single-strain model with waning immunity.

Data source	Hospitalization				GP consultation			
Model variant	(i)	(ii)	(iii)	(iv)	(i)	(ii)	(iii)	(iv)
Cost	0.1775	0.1779	0.0405	0.0332	0.0586	0.058	0.0358	0.0355
β	0.1882	0.0978	0.241	0.4341	0.3843	1.0174	0.176	0.1613
γ	0.0025	0.0284	0.1667	0.3705	0.0216	0.8754	0.0967	0.0856
δ_{summer}	-2.7718	-2.329	-0.4119	-0.1907	-2.519	0.0092	-0.7031	-0.6858
δ^{2009}_{winter}	0	1.2916	0	0.0801	0	0.2893	0	-0.0023
δ^{2010}_{winter}	0	1.2916	1.888	0.7288	0	0.2893	2.2956	3.1068
i_1	1.22e-05	0.0023	4.23e-05	3.87e-05	9.65E-012	5.73e-07	1.46e-04	2.21e-04
i_2	-5.72e-05	0.0012	-1.05e-05	1.80e-08	3.06e-04	1.98e-06	-2.36e-05	-4.71e-05

Table B.6: Best-fitting parameter sets for all four variants of the single-strain model without waning immunity.

Data source	Hospitalization				GP consultation			
Model variant	(i)	(ii)	(iii)	(iv)	(i)	(ii)	(iii)	(iv)
Cost	0.1299	0.0835	0.0402	0.0395	0.0422	0.0257	0.0361	0.0245
β	0.4766	0.4115	0.2311	0.2506	0.2196	0.5486	0.1752	0.6159
γ	0.3462	0.3551	0.1567	0.173	0.0575	0.4415	0.0953	0.4865
ω	0.0084	0.0048	0.0008	0.0008	0.0056	0.0024	0.0002	0.0034
δ_{summer}	-0.3693	-0.0611	-0.4287	-0.4501	-1.7835	-0.0622	-0.7634	0
δ^{2009}_{winter}	0	0.3631	0	0.0734	0	0.3032	0	0.3247
δ^{2010}_{winter}	0	0.3631	1.3405	1.5204	0	0.3032	1.7877	0.2086
i_1	3.06e-07	4.47e-04	5.09e-05	4.28e-05	5.91e-06	1.75e-05	1.52e-04	3.84e-06
i_2	2.80e-05	-2.85e-05	-1.13e-05	-5.31e-07	-3.00e-05	-6.20e-07	-3.42e-05	-2.33e-06

Appendix C. Parameter values for the two-strain model

Tables summarizing parameter values for the two-strain model are shown below, with all parameters explained on Table C.7. Table C.8 shows the best-fitting parameter sets for the two-strain model with waning immunity, fixed recovery and growth rates, and different assumptions for pre-existing immunities. The recovery rate was set to a biologically plausible value, $\gamma = 0.345$/day (13). The growth rate of the pandemic strain in the UK, $r_0^{UK} = \beta_1 (N_{SS} + \sigma N_{SR}) - \gamma = 0.0888$/day, was kept fixed by adjusting the infection rate of the pandemic strain, β_1.

Table C.7: Summary of model parameters for the two-strain model

Notation	Parameter	Value
β_1	Infection rate for the pandemic strain [1/day]	fixed
β_2	Infection rate for strain the seasonal strain [1/day]	estimated
γ	Recovery rate [1/day]	fixed
σ	Remaining susceptibility after first infection	estimated
δ_{winter}	Additional infection rate relative to base level for the winter months in 2009	estimated
δ_{sommer}	Additional infection rate relative to base level for the summer holidays in 2009	estimated
N_{AB}^X	Proportion of population initially in class $AB \in\in \{SS, SR, RS, RR\}$ in region $X \in \{US, UK\}$	all estimated, one estimated or fixed
i_1^X	Initial proportion of infectives in the beginning of 2009 spring wave (April 20) in region $X \in \{US, UK\}$	estimated
i_2^X	Initial proportion of infectives in the beginning of 2010 autumn wave (September 10) in region $X \in \{US, UK\}$	estimated
r_0^j	Initial growth rate for strain $j \in \{1, 2\}$	computed

Table C.8: Best-fitting parameter sets for the two-strain model with waning immunity, fixed recovery and growth rates, and different assumptions for pre-existing immunities.

Prior immunity	None	Only against H3N2	Only against H1N1	Against both strains
Cost	0.3287	0.0193	0.3157	0.0072
β_2	0.1475	0.9104	0.2709	1.2334
σ	0.9923	0.2411	0.7611	0.3748
ω	0.0016	0.0008	0.0016	0.0005
δ_{winter}	0.6864	0.4954	0.6123	0.7298
δ_{sommer}	-0.1216	-0.9272	-0.2898	-0.1625
N_{SR}^{US}	0	0.6042	0	0.6170
N_{RS}^{US}	0	0	0	0.1338
N_{RR}^{US}	0	0	0	0.1803
i_1^{US}	1.7511e-10	8.5348e-05	3.8916e-20	0.0050
i_2^{US}	0.0063	2.7356e-08	0.0014	7.4633e-05
N_{SR}^{UK}	0	0.7195	0	0.5316
N_{RS}^{UK}	0	0	0	0.0012
N_{RR}^{UK}	0	0	0	0.3349
i_1^{UK}	0.0011	8.5564e-05	4.6521e-04	3.1527e-05
i_2^{UK}	2.7558e-05	1.9609e-08	1.1503e-06	5.88846e-09